Available online at www.sciencedirect.com

ScienceDirect

Russian Geology and Geophysics 58 (2017) 1118–1128

RUSSIAN GEOLOGY AND GEOPHYSICS

www.elsevier.com/locate/rgg

Origin of false components of NRM during conventional stepwise thermal demagnetization

V.P. Shcherbakov [a,b,*], A.V. Latyshev [c,d], R.V. Veselovskiy [c,d], V.A. Tselmovich [a]

[a] *"Borok" Geophysical Observatory, Schmidt Institute of Physics of the Earth, Russian Academy of Sciences, Borok, Nekouz raion, Yaroslavl oblast, 152742, Russia*

[b] *Institute of Geology and Petroleum Technologies, Kazan (Volga) Federal University, ul. Kremlevskaya 18, Kazan, 420008, Russia*

[c] *Schmidt Institute of Physics of the Earth, Russian Academy of Sciences, ul. Gruzinskaya 10, Moscow, 123995, Russia*

[d] *Lomonosov Moscow State University, Geological Department, Leninskie Gory 1, Moscow, 119991, Russia*

Received 31 October 2016; received in revised form 19 January 2017; accepted 3 February 2017

Abstract

Many Permian–Triassic dolerite samples from the Siberian Trap Large Igneous Province exposed to conventional stepwise thermal demagnetization at 250–450 °C display mid-temperature remanence (MTC) directed opposite to the high-temperature NRM component. Alternating field (A.C.) demagnetization fails to isolate the antipodal component, but it appears during continuous thermal demagnetization, though in a different temperature range. Laboratory experiments and simulations prove that MTC remanence is an artifact resulting from magnetic memory of self-reversing titanomagnetite grains oxidized at low temperature. This effect can deform the results stepwise thermal cleaning and be responsible for misleading patterns of paleomagnetic directions. Given that oxidized titanomagnetite grains are widespread in volcanic rocks, we suggest to identify true paleodirections by combined continuous and stepwise thermal demagnetization. The extension of our model to the case of NRM_2 overprint directed at some angle to partially reversed primary NRM_1 component accounts for the difference between the results of stepwise and continuous thermal demagnetization observed in samples of the Steens Mountain basalt (USA).

Keywords: thermal demagnetization; magnetic memory; self-reversal; oxidized titanomagnetite; paleomagnetic directions

Introduction

Paleomagnetic directions are crucial to reconstructions of the morphology and history of the Earth's magnetic field and respective paleotectonic settings. Paleomagnetic studies stem from the assumption that natural remanent magnetization (NRM) in rocks aligns with the geomagnetic field at the time of rock formation. This postulate is valid in the first approximation but the situation is more complicated than that as the ultimate NRM vector is actually a sum of primary remanence and one or several secondary magnetization overprints. Thus, reconstructing the true direction of the past geomagnetic field requires removing the overprints, commonly by alternating field (A.C.) or stepwise thermal demagnetization, which destroys less stable NRM components and isolates the most stable one, assumed to be characteristic remanence (ChRM).

Conventional stepwise thermal demagnetization of a Miocene lava flow from Steens Mountain (USA) that presumably cooled during a geomagnetic polarity reversal revealed an unusual behavior of ChRM (Mankinen et al., 1985; Prévot et al., 1985). The ChRM direction in the 1.9 m thick lava flow B51 changes from bottom to top of the flow: it was parallel to the direction of the underlying flow B52 and then to that of the overlying flow B50. Actually, the paleodirections behaved in a more intricate way but we consider the main trend for simplicity. Possible causes of this change were largely discussed, for instance, in the overview by Coe et al. (2014), and the results of the conventional stepwise thermal demagnetization were found out to differ markedly from those of continuous cleaning. Below we provide details of the case reported by Coe et al. (2014) and discuss possible causes of the unusual ChRM behavior.

This study focuses on physical mechanisms that may lead to the discrepancy in results of stepwise and continuous thermal demagnetization. The observed effect is simulated in a phenomenological model based on rock-magnetic experiments. We suggest that the difference may be due to magnetic

* Corresponding author.
E-mail address: shcherbakovv@list.ru (V.P. Shcherbakov)

1068-7971/$ - see front matter
http://dx.doi.org/10.1016/j.rgg.2017.08.008

memory in titanomagnetite grains that experience low-temperature oxidation and are capable of partial self-reversal. The work was motivated by paleomagnetic data obtained for Permian–Triassic dolerite intrusions from the Siberian Trap Large Igneous Province. The standard procedure of stepwise thermal demagnetization revealed a high-temperature (HTC) and a viscous low-temperature (LTC) magnetization components, and quite many samples displayed also mid-temperature remanence (MTC), antipodal to HTC. The details have been reported elsewhere (Latyshev et al., in revision) and are not considered in this paper. The question arises whether the mid-temperature remanence present in many samples marks geomagnetic reversal during or after the intrusion event or it is an artifact produced by some specific rock magnetic properties. To solve the problem, we undertook paleomagnetic studies along with thermomagnetic and electron microprobe analyses.

Note that a similar effect was discovered recently in 214 Ma basalts sampled from the Rochechouart impact crater in France where the reversed component appeared in the 425 to 625 °C temperature range of thermal cleaning (Eitel, 2014).

The presence of antipodal remanence, in a single "anomalous" sample or within a lava flow, was quite often reported from the Siberian Trap Province (Fetisova et al., 2014; Mikhaltsov et al., 2012; Veselovskiy et al., 2003). The effect has been usually attributed to self-reversal (Fetisova et al., 2014; Veselovskiy et al., 2003) but has almost never been reproduced in laboratory, with a few exceptions.

Similarity with the Steens Mountain case (Coe et al., 2014) made us look more closely into the problem of discrepancy between the results of stepwise and continuous thermal demagnetization.

Methods

Thermal demagnetization of samples was performed at paleomagnetic laboratories of the Institute of Physics of the Earth and Geological Institute of the Russian Academy of Sciences and at Moscow University (all in Moscow), following the standard procedure (Khramov et al., 1982; Shipunov, 1999; Zijderveld, 1967). The external magnetic field was compensated using a magnetically shielded room or a Helmholtz coil system.

Thermomagnetic and electron microprobe analyses were run at the Borok Geophysical Observatory (Borok, Yaroslavl region). In order to estimate the Curie temperatures (T_c) and thermal stability of ferrimagnetic minerals, we recorded temperature-dependent saturation magnetization $M_s(T)$ on magnetic scales, in a constant external magnetic field of 0.45 T. The Curie temperatures were determined according to peaks of the first derivative on the $M_s(T)$ curve following recommendations of Fabian et al. (2013). Continuous thermal demagnetization was performed on a three-component vibrating thermomagnetometer of the sensitivity 10^{-8} Am^2 designed by Yu.K. Vinogradov.

The composition of ferrimagnetic minerals was analyzed on a TESCAN *VEGA II LMU* scanning electron microscope (Czech Republic) with an Oxford Instruments Energy 450 detector.

Samples

We collected 350 oriented samples from thirty five trap intrusions widespread in the Lower Tunguska Valley (Fig. 1). The intrusions are mostly sills, or less often dikes and stocks, composed mainly of fine- and medium-grained dolerite. They

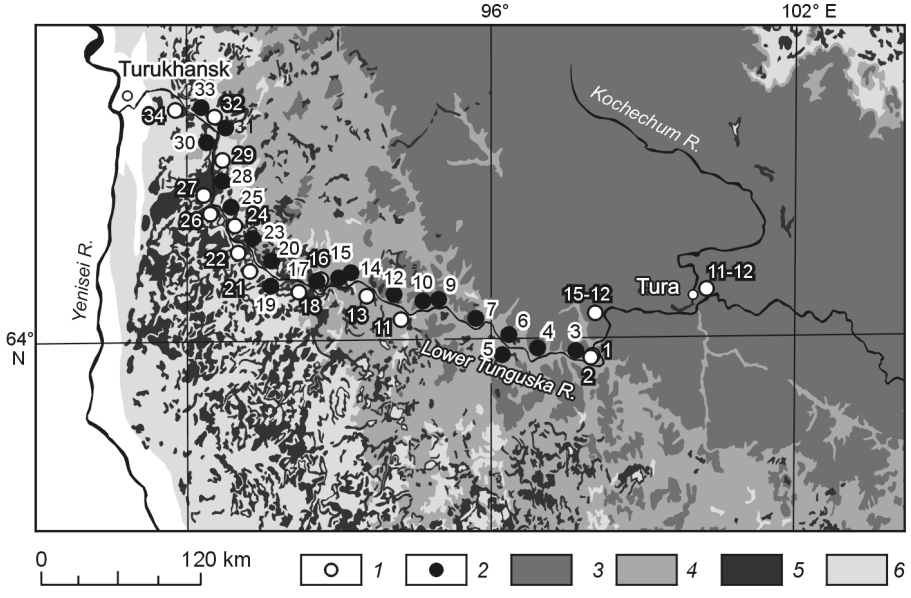

Fig. 1. Simplified geology of the study area. *1*, *2*, Paleomagnetic sites with one stable HT component (*1*) and two antipodal components (*2*); *3*, *4*, Permian–Triassic traps, mainly lavas (*3*), and tuffs (*4*); *5*, intrusions; *6*, Paleozoic sediments on Siberian craton.

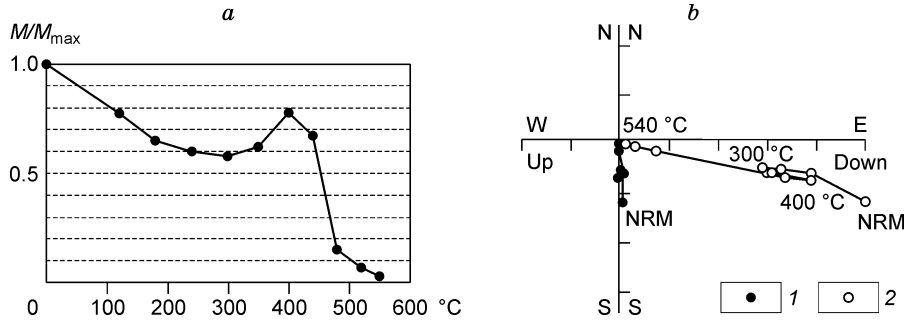

Fig. 2. Results of stepwise thermal demagnetization of sample 25 (with antipodal mid-temperature remanence, site 3 in Fig. 1). *a*, Change of $NRM_s(T)$; *b*, change of $NRM_s(T)$ direction with temperature. Reversed MTC appears in the 300–400 °C range. *1*, *2* are horizontal (*1*) and vertical (*2*) projections.

emplaced in Upper Paleozoic sedimentary host rocks of the Siberian craton in the western part of the study area and in Permian–Triassic tuff and lavas in the east. According to published U–Pb ages, the Lower Tunguska sills formed in the earliest Early Triassic: 251.795 ± 0.070 and 251.786 ± 0.054 Ma for sills in the lower reaches of the Lower Tunguska; 251.74 ± 0.18 Ma for an intrusion 150 km east of Tura Village (Burgess and Bowring, 2015).

Demagnetization results

Stepwise thermal demagnetization was applied to all dolerite samples from the thirty five paleomagnetic sites in the Lower Tunguska valley. Samples from sixteen sites showed standard two-component NRM: low-temperature, possibly, viscous remanence (LTC) destroyed at 200–300 °C and high-temperature remanence (HTC) unblocked at 600 °C, identified as the characteristic component (ChRM). Besides the high- and low-temperature components, NRM of samples from nineteen sites, contained mid-temperature remanence (MTC) directed antipodally to HTC, detectable within large temperature ranges from 240–450 °C to 400–540 °C and 530–590 °C at different sites.

The mid-temperature remanence was observed in about one third of stepwise demagnetized samples of the collection. As shown in Fig. 2, low-temperature viscous remanence is unblocked at 200 °C; then NRM decreases upon further heating, while points in the Zijderveld diagrams drift to the origin of coordinates (hereafter NRM_s and NRM_c refer, respectively, to stwepwise and continuous cleaning); at 300 °C, $NRM_s(T)$ begins growing, while the points in the orthogonal diagram shift back. The sample becomes fully demagnetized as HTC has been unblocked above 400 °C. Such cleaning patterns are commonly attributed to the presence of reversed mid-temperature remanence at 300–400 °C.

Table 1. Results of reversal test for sites with antipodal remanence component

Site	HTC polarity	*N*, HTC/MTC	γ/γ_{cr}, deg
3	N	10/10	2.4/3.5
4	N	10/5	2.0/4.6
9	N	12/9	3.9/4.6

Note. *N* is the number of samples used to calculate average direction; HTC is the high-temperature remanence; MTC is the mid-temperature remanence; γ/γ_{cr} is the ratio of angular distance between HTC and MTC to critical angle, after (McFadden and McElhinny, 1990).

The antipodal directions of HTC and MTC were checked by the reversal test (McFadden and McElhinny, 1990) for samples from three sites, where the mid-temperature component is reliably detectable at 240–450 °C in at least five samples from a site. The results (Table 1) show that the angle γ between the directions does not exceed the critical angle γ_{cr}, i.e., the test result is positive.

Stepwise demagnetization by alternating magnetic field was performed for six samples containing antipodal MTC. The NRM vector in all samples comprised (Fig. 3) a low and a high coercive remanence components. The low coercive component was removed at 5–10 mT and may be viscous, while the high one was unblocked within 10–80 mT in all samples and had the same polarity as HTC. No antipodal components like those in the case of thermal demagnetization were observed.

Continuous thermal demagnetization was applied then to the same six samples. The respective $NRM_c(T)$ curves lack antipodal MTC revealed at $NRM_s(T)$ of 350–400 °C during the stepwise thermal cleaning (solid line in Fig. 4*a*). On the other hand, the $NRM_c(T)$ curve (dashed line in Fig. 4*b*) contained a reverse (self-reversed) component (SRC) at low temperatures of $T < 150$–200 °C.

Thus, both stepwise and continuous thermal demagnetization reveal the antipodal component but at markedly different temperature ranges. In order to understand the causes of this discrepancy, we recorded temperature curves NRM(T) at heating to progressively higher temperatures T_i (Fig. 5).

Heating to 350 °C led to a slight drift and decrease of the peak the NRM(T) curves reach between 100 and 150 °C (Fig. 5*a*), but it did not unblock the self-reversed component SRC(T_i) corresponding to difference between the peak and room-temperature NRM intensities. As shown by experiments, unblocking of SRC(T_i) begins at 400 °C and higher (Fig. 5*b* and 5*c*). The NRM drift and reduction obviously result from unblocking of low-temperature remanence, including its viscous portion. Thus, our experiments reveal at least two

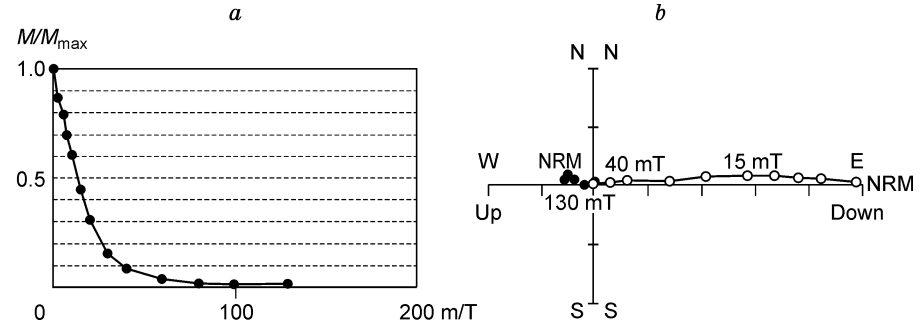

Fig. 3. Results of A.C. demagnetization of sample 26 (Fig. 1, site 3). No traces of antipodal MTC which was isolated by stepwise thermal demagnetization. *a*, Change in NRM intensity; *b*, direction change. For symbols see Fig. 2.

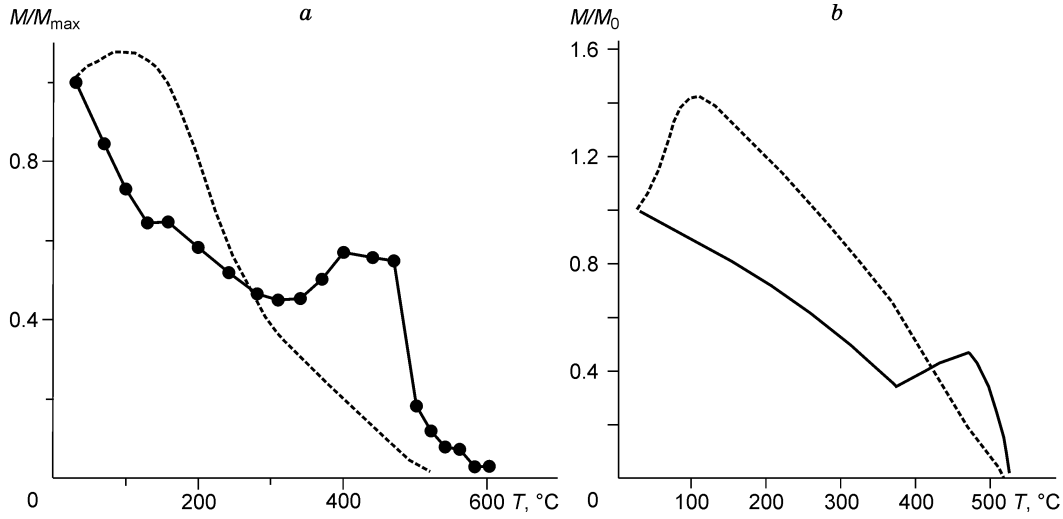

Fig. 4. *a*, Curves of continuous (dash line) and stepwise (solid line) thermal demagnetization of sample 26 (with MTC). Thermomagnetic curves are recorded on identical samples with primary NRM. *b*, Respective calculated curves of stepwise and continuous demagnetization of normalized NRM.

different NRM components: one normal and one self-reversed (at $T < 150$ °C). However, it remains unclear why the low-temperature reversed component becomes unblocked only above 400 °C. The physics of this unusual behavior is discussed in the following sections.

Thermomagnetic analysis

Curves of temperature-dependent saturation magnetization $M_{si}(T)$ are of three thermomagnetic types. In *A*-type $M_{si}(T)$ curves (Fig. 6*a*), $T_c \approx 150$–200 °C but a long "tail" extends to 500–600 °C. Curve shapes change notably upon heating to 500 °C and higher, at decreasing low-temperature phases and increasing high-temperature ones with Curie temperatures reaching 600 °C. This behavior of $M_{si}(T)$ curves records low-temperature oxidation on surfaces of primary titanomagnetite grains induced by heating, whereby M_s slightly decreases and T_c increases.

Very stable $M_s(T)$ curves of type *B* (Fig. 6*b*) remain almost invariable upon heating while the Curie temperature of samples is about that in magnetite. Unlike type *B*, heating to 600 °C in the case of type *C* (Fig. 6*c*) decreases the saturation magnetization of samples and leads to the formation of a relatively low-temperature phase with $T_c \approx 300$–350 °C. This phase forms ever more rapidly upon repeated heating to 700 °C (dashed line). This pattern suggests the presence of spinodal decomposition structures in primary titanomagnetites and their subsequent homogenization as the samples are heated to above the spinodal temperatures (600 °C in this case) leading to recovery of the titanomagnetite phase with a relatively low T_c.

Curves in Fig. 6*a* correspond to samples with a self-reversed mid-temperature remanence which became subject to further analysis. Those of Fig. 6*b* are typical of samples with a single NRM component. A weak reversed component appears also at stepwise thermal demagnetization of samples with $M_s(T)$ of the type of Fig. 6*c*, but at much higher temperatures of ≈ 530–570 °C. It may result from mineralogical changes in spinodal decomposition structures, but this problem is beyond the present consideration and requires a separate study. Note only that this range of high temperatures is close to that of the reversed remanence in basalts from the Rochechouart impact crater (Eitel, 2014).

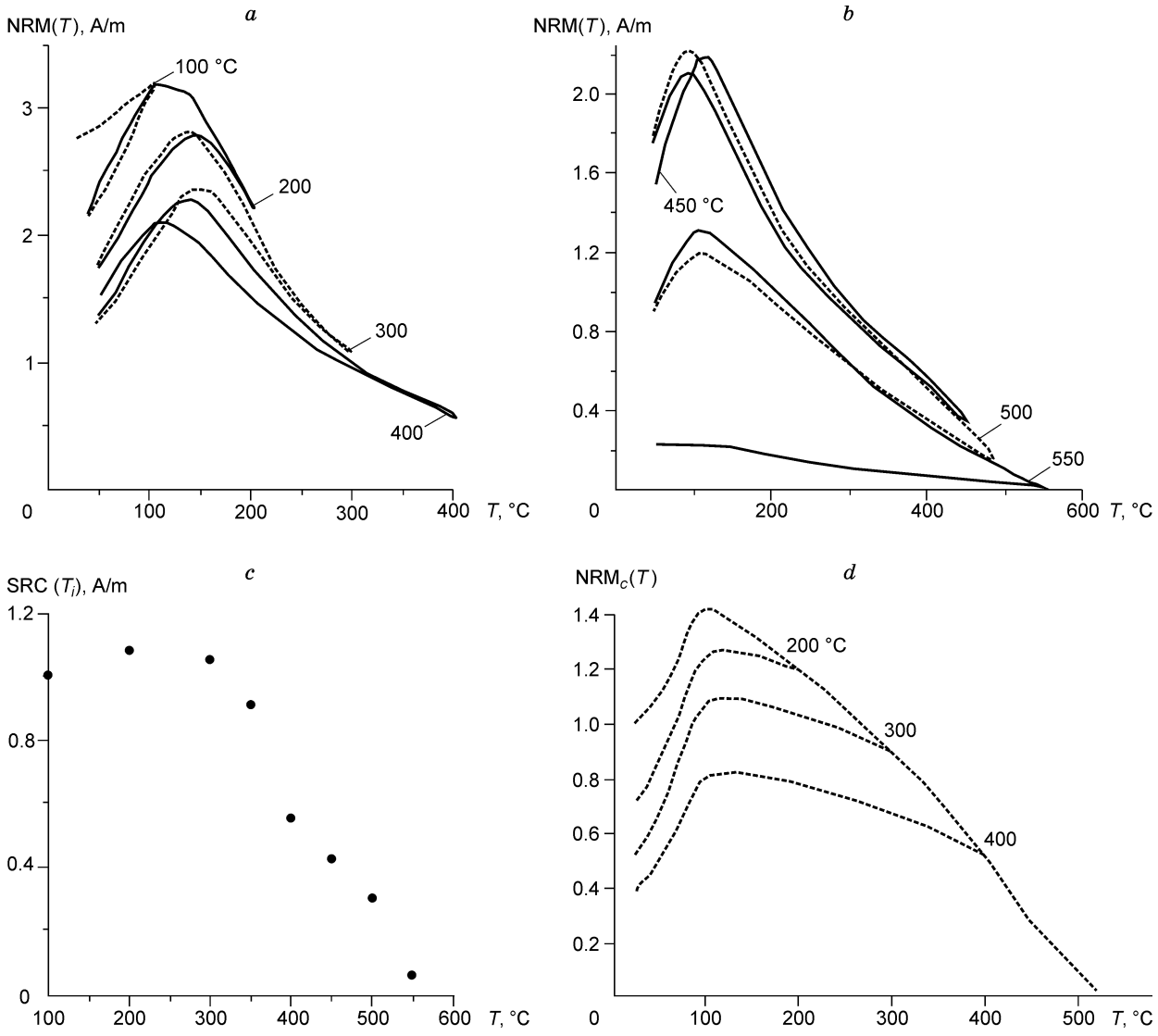

Fig. 5. Thermomagnetic demagnetization curves at stepwise heating to progressively higher temperatures. Sample 25 (with MTC). *a*, Heating/cooling cycles to temperatures T_i: $T_1 = 100$; $T_2 = 200$; $T_3 = 300$; $T_4 = 400$ °C; *b*, same for $T_5 = 450$; $T_6 = 500$; $T_7 = 550$ °C; *c*, intensity of SRC (T_i); *d*, simulation of $NRM_c(T)$ thermal demagnetization curves at heating to $T_i = 200$, 300, 400, 520 °C, calculated for $S = 4$, $b = 5$, $b_0 = 1$, $p = 0.5$, $q = 1$, $T_{cA} = 750$ K, $T_{cB} = 400$ K, $T_{low} = 400$ K, $T_{c2} = 750$ K, $T_{12} = -2$ K.

Electron microprobe analysis

Electron microprobe analysis of a thin section of sample 25 (thermomagnetic type *A*, with antipodal MTC) which showed a reversed NRM component during thermal demagnetization, revealed titanomagnetite grains with $x \approx 0.6$–0.7, sometimes adjacent to grains of pure ilmenite (Fig. 7*a*). Titanomagnetite of this composition has $T_c \approx 150$ °C, which is consistent with thermomagnetic data. XRD confirmed the presence of spinel with a lattice constant of a = 0.847–0.848 nm, which corresponds to weakly oxidized titanomagnetite with $x \approx 0.6$ (Nishitani and Kono, 1983).

On the other hand, electron microscopy detected grains (or grain sites) that underwent notable low-temperature ("single-phase") and/or high-temperature ("heterophase") oxidation judging by irregular, curved cracks (Fig. 7*b*) which are typically associated with low-temperature oxidation, as reported for ocean floor titanomagnetite (Petersen, 1987). Oxidation is especially prominent at sites around cracks (Krása et al., 2005). The grain shown in Fig. 7*c* experienced oxidation-driven exsolution producing magnetite and ilmenite lamellae. The micron-size and coarser lamellae originated at temperatures as high as >700 °C (Gapeev and Tselmovich, 1988) while submicron lamellae (visible in the same figure) trace a continuing process of high-temperature oxidation as far as $T \approx$ 550–600 °C. These lamellae, along with low-temperature-oxidized grains (or grain sites), may be responsible for the long tails with high Curie temperatures in the $M_S(T)$ curves of Fig. 6*a*.

Discussion

Magnetic memory. The magnetic-mineralogical and electron microscopy data show quite a complex mineralogy of

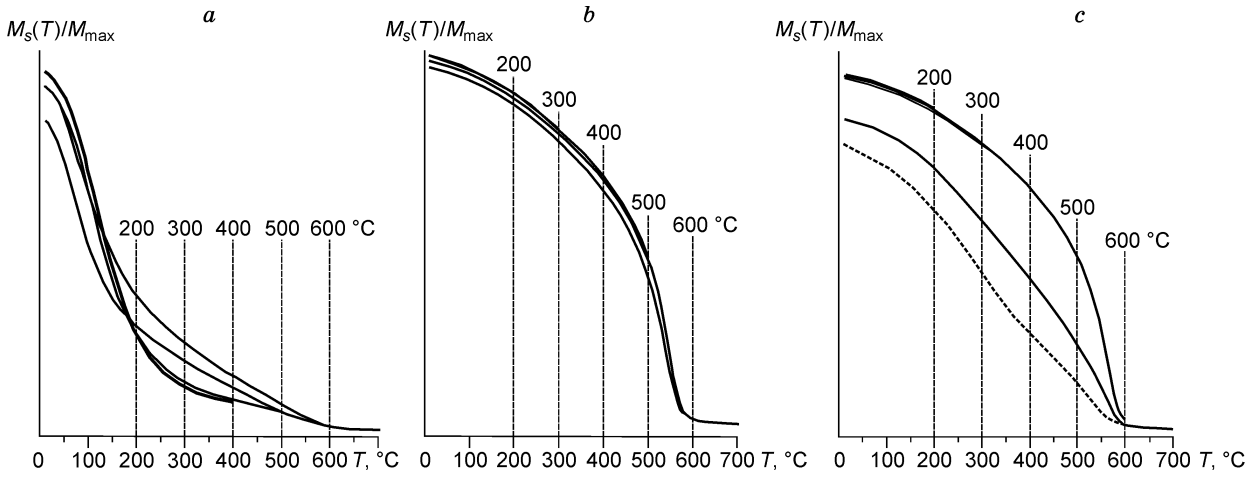

Fig. 6. Typical temperature-dependent behavior of saturation magnetization $M_{si}(T)$ (a.u.) at stepwise heating to progressively higher T_i. *a*, Sample 25 , type *A* (site 3, stepwise thermal demagnetization reveals only MTC in the range 250–450 °C); *b*, sample 258, type *B* (site 24, stepwise thermal demagnetization reveals only HTC); *c*, sample 268, type *C* (site 25, stepwise thermal demagnetization reveals only MTC in the range 530–570 °C). Vertical lines correspond to maximum temperatures at each heating step.

samples that demonstrate the presence of a false reversed NRM component. Namely, they contain titanomagnetite with $T_c \approx 150$–200 °C and ulvospinel of $x \approx 0.6$; have low-temperature oxidized sites with a large range of Curie temperatures extending to $T_c = 500$ °C and higher; finally, they bear deuterically oxidized multiphase titanomagnetite with ferrimagnetic unit-cell sizes close to pure magnetite. This mineralogy is almost identical to those of basalts that displayed self-reversed magnetic remanence as described by Krása et al. (2005). In that case, titanomagnetite was present in two magnetic phases: a nonoxidized magnetically soft phase with Curie temperatures $T_c \approx 200$ °C and a magnetically hard low-temperature oxidized part with T_c = 400–500 °C (Krása et al., 2005). It is the magnetic coupling of the two phases (it remains unclear whether it is exchange or magnetostatic interactions) that is responsible for the self-reversed remanent magnetization of the low-temperature phase at $T < 150$–200 °C, i.e., below the T_c of primary titanomagnetite.

Proceeding from this analogy, nonhomogeneously oxidized titanomagnetite must be the carrier of self-reversed remanence. Hemoilmenite ($Fe_{2-y}Ti_yO_3$, $y \approx 0.5$) could be another candidate in this respect, but the XRD patterns reveal only a rhombic phase with a unit-cell size corresponding to pure ilmenite, without any traces of hemoilmenite. The idea of oxidized titanomagnetite as a carrier of self-reversed remanence is supported by experimental evidence of Krása et al. (2005), whose thermal demagnetization experiments, performed in similar way to our experiments, have shown that the thermomagnetic curves obtained here and there are perfectly congruent (cf. Fig. 3 in (Krása et al., 2005) and our Fig. 5). Thus, the question is why the presence of a mineral capable of low-temperature self-reversal leads to strikingly different results in stepwise and continuous thermal demagnetization.

This discrepancy can be explained in terms of the magnetic memory theory implying that grains of the low-temperature phase in a two-phase system can "memorize" their primary direction due to magnetic coupling of phases and can recover this direction after thermal demagnetization as the sample cools down to below its Curie temperature T_{cB} (Prévot et al., 2001). If NRM forms by two coupling phases with markedly different Curie temperatures, loss of magnetic memory, i.e., demagnetization of the low-temperature phase measured at the room temperature T_r, is possible only by unblocking of high-temperature grains. In our case, the range of unblocking temperatures (T_{ub}) of the high-temperature phase extends as far as $T_{cA} \approx 550$ °C. Thus, the remanence of the low-temperature phase always recovers, fully or partially, during stepwise demagnetization upon cooling from temperatures not exceeding T_{cA}. This simple idea provides a natural explanation for the appearance of the reversed mid-temperature remanence during stepwise thermal demagnetization. It is clear that, with this mechanism, the temperatures of MTC formation falls within the range of unblocking temperatures for HTC. Thus, heating to below this range unblocks neither the primary component nor the reversed one which can be removed only together with the primary component when the sample reaches the respective temperatures (≈ 400 °C). This shows up in the Zijderveld diagrams as the presence of a reversed NRM component in the mid-temperature range. On the other hand, continuous demagnetization first unblocks the self-reversed low-temperature remanence (which is recorded in the rise of temperature curves at $T < 150$ °C in Figs. 4, 5), and only then NRM(T) decays monotonically as the magnetic moments of the unblocked grains become released and the spontaneous magnetization (M_s) of the high-temperature phase decreases. Note that M_s of the low-temperature phase *B* at these temperatures becomes zero and causes no influence on the NRM(T) curve at $T > T_{cB}$.

Simulation of reversed MTC. According to the mineralogy of the samples, we assume two-phase titanomagnetite to be the carrier of the NRM_1 component (Fig. 8). The two

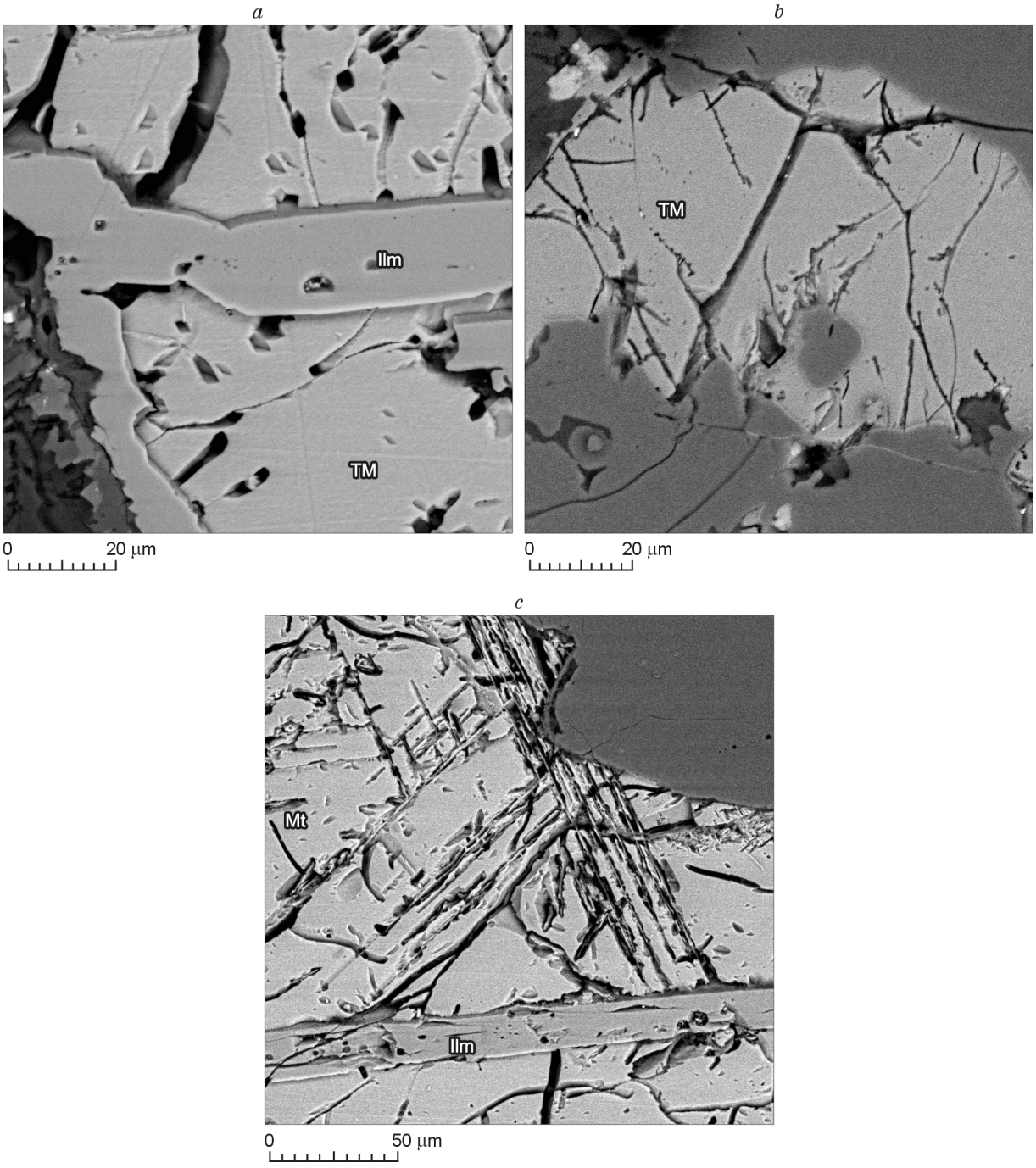

Fig. 7. Microphotographs of sample 25 (displaying mid-temperature remanence). *a*, Grain of titanomagnetite (TM) of the composition $x = 0.6$ with ingrown ilmenite (Ilm); *b*, systems of cracks typical of low-temperature oxidized grains; *c*, two-stage oxidation of different phases: a large lamella below and thin submicron lamellae above. Mt is magnetite.

phases are a stoichiometric titanomagnetite matrix (phase *A*) and strongly oxidized inclusions (phase *B*).

The component NRM_2 is normal, free from any singularities. In the applied formalism, it is presented by a ferrimagnetic single phase with the Curie temperature T_{c2}. For certainty, we assume also that NRM_1 and NRM_2 are thermomagnetic. Then, the general equation for $NRM_k(T, T_b)$ (k = 1, 2) at cooling to room temperature in the low external field h is given by

$$\mathrm{NRM}_k(T_r) = h \int_{T_r}^{T_c} \frac{y_k(T)}{y_k(T_b)}\, c_k(T_b)\, \chi_k(T_b)\, dT_b. \qquad (1)$$

The factor $y_k(T)/y_k(T_b)$ accounts for temperature-dependent ordering changes $y_k(T) = M_{sk}(T)/M_{sk}(0)$, where $M_{sk}(T)$ is the spontaneous magnetization of a given grain, χ_k is its paramagnetic susceptibility, and $c_k(T_b)$ is the relative volumetric concentration of grains with the blocking temperature T_b. Let

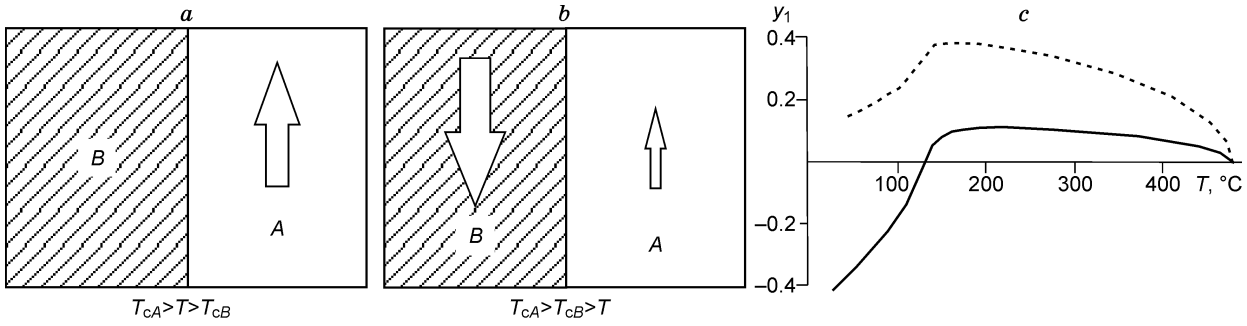

Fig. 8. Panels *a* and *b* illustrate a two-phase model for a titanomagnetite grain in different temperature ranges; panel c shows temperature dependence of normalized spontaneous magnetization. Size of arrows is proportional to magnetization at $S = 4$; $T_{cA} = 400$ K; $T_{cB} = 750$ K; $T_{12} = 2$ K, $b = 1$ (dashed line), $b = 5$ (solid line). Calculated with equations (6) and (7).

$p(T_b, T_{ub})$ be the probability of unblocking upon heating to $T = T_{ub}$. Introducing this probability distribution function is necessary because the blocking and unblocking temperatures are identical only in the case of single-domain grains (Shcherbakova et al., 2000). Then the total remanence normalized to h, measured as the sample is heated to the temperature T, is

$$\mathrm{NRM}_k(T)\uparrow = y_k \int_T^{T_c}\int_{T_r}^{T_c} \frac{c_k(T_b)\chi_k(T_b)}{y_k(T_b)} p_k(T_b, T_{ub})\, dT_b\, dT_{ub}$$

$$= y_k(T)\, F_k(T). \qquad (2)$$

$F_k(T)$ is the cumulative spectrum introduced for convenience:

$$F_k(t) = \int_T^{T_c}\int_{T_r}^{T_c} \frac{c_k(T_b)\chi_k(T_b)}{y_k(T_b)} p_k(T_b, T_{ub})\, dT_b\, dT_{ub}. \qquad (3)$$

Unlike continuous thermal demagnetization, heating to some intermediate temperature T in the stepwise procedure is followed by cooling back to room temperature T_r. Therefore, (2) becomes

$$\mathrm{NRM}_k(T)\uparrow\downarrow = y_k(T_r)\, F_k(T). \qquad (4)$$

Equations (2) and (4) express the continuous and stepwise thermal demagnetization curves in a simple and clear way, in terms of the order parameter $y_k(T)$ and the cumulative spectrum of unblocking temperatures $F_k(T)$. From the derivation it is evident that the equations are valid irrespective of the NRM nature, whether it is thermal, chemical, or thermochemical remanence.

The order parameter $y_k(T)$ is very hard to exactly estimate, even in the molecular field approximation (Fabian et al., 2015), because titanomagnetite is a ferrimagnetic mineral in which each ion is involved into exchange with a large number of nearest and next ions. However, the details of its behavior are irrelevant for the present problem, while $y_2(T)$ can be calculated using the simple Weiss theory implying that (Vonsovskiy, 1971)

$$y_2 = B_S\left(\frac{T_{c2}}{T}\frac{3S}{S+1}\, y_2\right),\ B_S(x) = (2S+1)/(2S)\coth((2S+1)x/(2S)) - \coth\,(x/(2S))/(2S), \qquad (5)$$

where $B_S(x)$ is the Brillouin function and S is the spin. Note also that all temperatures in this section are quoted in Kelvin unless noted otherwise.

Since the NRM_1 carriers have complex compositions, the average order parameter is used:

$$y_1 = (v_A y_A + v_B\, y_B)/(v_A + v_B) = (y_A + b y_B)/(1+b), \qquad (6)$$

where v_A and v_B are the volumes of phases A and B, respectively, and y_A and y_B are their order parameters. The coefficient $b = v_B/v_A$ is the volume ratio (relative volumes) of the phases A and B. The functions y_A and y_B can be calculated, in the first approximation, likewise using the Weiss theory (5) but with an added term corresponding to their negative exchange or magnetostatic interaction. This interaction can be taken into account with an approach suggested by Néel (Vonsovskiy, 1971) for describing ferrimagnetism, using the standard system of two equations:

$$y_A = B_S\left[\frac{3S}{S+1}\left(\frac{T_{cA}}{T}\, y_A + \frac{T_{12}}{T}\, y_B\right)\right],$$

$$y_B = B_S\left[\frac{3S}{S+1}\left(\frac{T_{cB}}{T}\, y_B + \frac{T_{12}}{T}\, y_A\right)\right]. \qquad (7)$$

Note that in the case of weak interaction $T_{12} \ll T_{cA}$ and $T_{12} \ll T_{cB}$ we use for our calculations, the true T_{12} value almost does not affect the result. Under this condition, negative interaction only provides the antiparallel position of the vectors $\mathbf{M}_{sA}$ and $\mathbf{M}_{sB}$ required for partial or full reversal.

Of course, this model is far from reality, and the spatial distribution of ordering in nanoparticles should be rather calculated in terms of micromagnetic equations for two-phase nanoparticles as it was done in (Shcherbakov et al., 2012; Wang and Mills, 1992). Specifically, the model is disadvantageous in the case of magnetostatic interaction because equation (7) does not account for heterogeneity of the interaction field with respect to the phase volume. On the other hand, exchange is restricted to phase boundaries, which requires a separate approach. However, this problem is far

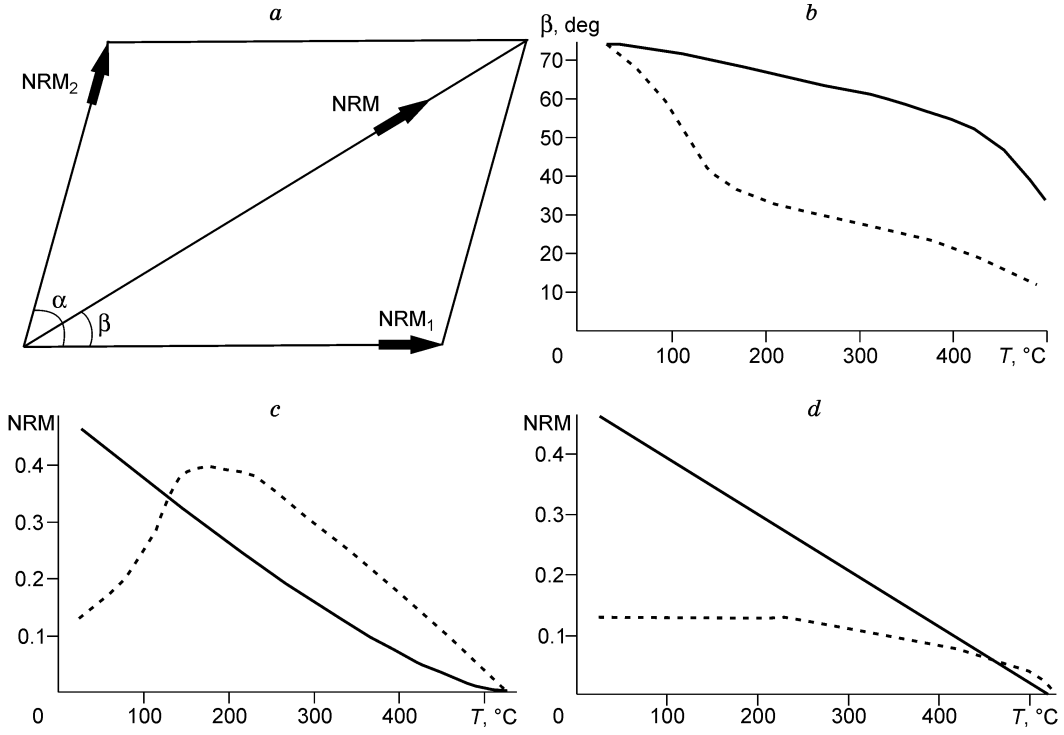

Fig. 9. *a*, Relative positions of NRM, NRM_1 and NRM_2 vectors; *b*, temperature (ºC) dependence of angles β_s (solid line) and β_c (dashed line); *c*, temperature-dependent NRM_2 (solid line) and NRM_1 (dashed line) at continuous thermal demagnetization; *d*, same, for stepwise cleaning. Magnetization is quoted in arbitrary units (a.u.); model parameters: $T_{c2} = 800$ K; $T_{cB} = 800$ K; $T_{cA} = 400$ K; $T_{low} = 500$ K; $T_{12} = -2$ K, $\alpha = /2$; $b = 1$; $b_0 = 0.5$; $p = 1$; $q = 0.5$.

beyond the scope of this study focused mainly on qualitative explanation of the observed effect, on the basis of the above physical principles rather than process details.

The curve $y_1(T)$ for two different weight ratios of normal and reverse components (Fig. 8*c*) shows that complete NRM_1 reversal, as expected, arises at predominant contribution of reversed remanence when its total volume strongly exceeds the normal one ($b \gg 1$).

As it follows from (3) and (4), completion of the calculations requires assuming the temperature dependence $F_1(T)$ and $F_2(T)$. According to equation (2), $F_1(T)$ corresponds to the experimental continuous thermal magnetization curve NRM(T), accurate to the factor $y_1(T)$. In the same way, the spectrum $F_2(T)$ corresponds to the curve of stepwise demagnetization NRM(T), to $y_1(T_r)$. Viewed in more detail, the curves in Figs. 2 and 4 show that temperature-dependent NRM decrease is more or less uniform over the whole temperature range (T_r, T_{c0}). Therefore, we assume that the blocking temperatures of normal remanence are present in this range. For convenience of calculations, we introduce the non-dimensional spectra $f_1(T) = F_1(T)/F_1(T_r)$ and $f_2(T) = F_2(T)/F_2(T_r)$. Proceeding from the above considerations, for simplicity, the power approximation $f_2(T) = ((T_{c2} - T)/(T_{c2} - T_r))^p$ is used below. On the other hand, stepwise thermal demagnetization experiments show that the reversed component has a relatively narrow range of blocking temperatures in the region adjacent to T_{cA}. Let T_{low} be the lower bound of this range; then, assume that $f_1(T) = 1$ if $T < T_{low}$ and $f_1(T) = ((T_{cA} - T)/(T_{cA} - T_{low}))^q$ if $T \subset (T_{low}, T_{cA})$. Hereafter p, q and T_{low} are fitting parameters.

With the total $nrm(T) = (NRM_1 + NRM_2)/F_1(T_r)$, at $b_0 = F_2(T_r)/F_1(T_r)$, it follows from (2) and (4) that

$$NRM_c(T) = y_1(T) f_1(T) + b_0 y_2(T) f_2(T),$$
$$NRM_s(T) = f_1(T) + b_0 f_2(T). \quad (8)$$

The NRM_c and $NRM_s(T)$ remanence curves (dashed and solid lines, respectively, in Fig. 4*b*) calculated with the chosen parameters agree quite well with the experimental curves.

Finally, simulation results for NRM(T) curves at heating to progressively higher temperatures (Fig. 5*d*) are compared with the respective curves of Fig. 5*a* and 5*b*, and again good agreement is observed.

Simulation of continuous and stepwise thermal demagnetization of Steens Mountain basalt. This section deals with causes of discrepancy in results of continuous and stepwise thermal demagnetization applied to the Steens Mountain Miocene lava samples. According to the first, quite exotic, hypothesis the remanent magnetization of a lava flow (B51) recorded extraordinarily fast field change in a week while lava was cooling during a geomagnetic polarity reversal (Prévot et al., 1985).

A more realistic explanation consists in baking by the erupting overlying flow B50, whereby the B51 rocks acquired secondary magnetization NRM_2 parallel to the B50 direction. The overlap of the ranges of NRM_2 and NRM_1 unblocking temperatures in stepwise thermal demagnetization leads to the formation of intermediate high-temperature directions ob-

served after thermal demagnetization to 500 °C (Coe et al., 1995). To test this hypothesis, Coe et al. (2014) performed a series of experiments including continuous thermal demagnetization. The results showed ChRM directions in B51samples to align with that in the underlying flow B52. Nevertheless, the causes of the observed discrepancy remained unclear. Coe et al. (2014) suggested chemical alteration associated with stepwise cleaning, but the difference in heating rates between the two procedures is insufficient to make the reaction temperature at least one hundred degrees hotter.

We applied our model to explain the stepwise and continuous thermal demagnetization results for the Steens Mountain basalt, being motivated by two facts. First, the flow B51 contains two ferrimagnetic phases with $T_c \approx 100$ and 475 °C, with a minor amount of magnetite (Coe et al., 2014), like our samples displaying MTC. Second, the results of stepwise and continuous thermal demagnetization of B51 samples were different, as in our case. Both facts naturally make thinking about similarity of physicochemical processes in the Steens Mountain and Siberian samples.

Assume that the total NRM vector is a sum of two noncollinear components NRM_1 and NRM_2, where partially self-reversing oxidized titanomagnetite is the carrier of primary NRM_1. According to the experimental data of Coe et al. (2014), NRM_1 aligns with the remanence of the underlying lava flow B52 while NRM_2 is acquired by reheating during eruption of the upper flow B50 and, correspondingly, aligns with its direction. The normal-polarity phase may be secondary titanomaghemite after titanomagnetite or undetected submicron particles of titanomaghemite or another magnetic phase (Coe et al., 2014).

Assume, without loss of generality, that the vectors NRM, NRM_1 and NRM_2 lie in the plane (x, y) and that NRM_1 is directed along the x axis. Then, the total magnetization vector ($NRM = NRM_1 + NRM_2$) during continuous thermal cleaning is at the angle $\beta_c(T)$ to this axis:

$$\beta_s(T) = \arctan \frac{(\sin\alpha)\,NRM_{2s}(T)}{NRM_{1s}(T) + (\cos\alpha)\,NRM_{2s}(T)}. \quad (9)$$

In the same way, during stepwise thermal demagnetization:

$$\beta_c(T) = \arctan \frac{(\sin\alpha)\,NRM_{2c}(T)}{NRM_{1c}(T) + (\cos\alpha)\,NRM_{2c}(T)}. \quad (10)$$

The functions $NRM_{1c}(T) = y_1(T)f_1(T)$, $NRM_{2c}(T) = b_0y_2(T)f_2(T)$ and $NRM_{1s}(T) = y_1(T_r)f_1(T)$, $NRM_{2s}(T) = b_0y_2(T_r)f_2(T)$ refer to the intensities of the self-reversed and normal components during the continuous and stepwise thermal cleaning, respectively.

At the chosen modeling parameters, the NRM vector originally lying at $\beta \approx 80°$ is directed very close to the NRM_2 component. During cleaning, with any method, it turns toward the primary component NRM_1 (Fig. 9*b*) because both angles β_c and β_s decrease with temperature. However, it rotates slowly and reaches $\beta_s \approx 45°$ in the case of stepwise demagnetization but its rotation in the case of continuous demagnetization, first rapid and then gradual, brings it to $\beta_c \approx 10°$, or close to NRM_1. This behavior generally coincides with that reported by Coe et al. (2014) and is consistent with their inference of misleading directions for B51 from stepwise demagnetization but almost true directions provided by continuous demagnetization.

Physically, the difference is due to the presence of a partially self-reversed ferrimagnetic phase in the samples. Indeed, temperature-dependent direction variations are controlled by the respective changes in the intensities of the constituent remanence vectors NRM_1 and NRM_2, as it follows from equations (9) and (10). Note that they behave in different ways: NRM_2 decreases monotonically during heating (solid line in Fig. 9*c*, *d*) whereas NRM_1 (dashed line) is low at room temperature as a result of partial self-reversal (fractions of NRM_2) but increases rapidly during continuous heating and markedly exceeds NRM_2 already at 200 °C as the reversed phase *B* becomes demagnetized (Fig. 8). This fact, along with further increase in NRM_1 relative to NRM_2 (Fig. 9*c*), is responsible for the final rotation of NRM toward NRM_1.

However, NRM_1 remains low due to magnetic memory during stepwise demagnetization until the high-temperature normal phase *A* begins to lose magnetization (Fig. 9*d*). As a result, the NRM vector remains close to NRM_2 and turns slowly toward NRM_1 only at higher temperatures $T > 400$ °C, when NRM_2 decreases notably. At the same time, NRM_1 decreases as well because this temperature range already reaches the unblocking temperatures of the phase *A*. Therefore, the final direction depends on details of decay in both components. In the case of Fig. 9, NRM stops at some intermediate position.

Conclusions

1. The antipodal mid-temperature remanence (MTC) revealed by the conventional stepwise thermal demagnetization of Permian–Triassic dolerites from the Siberian Trap Province is an artifact resulting from self-reversed remanence overprinting the normal component.

2. The phenomenological model of stepwise and continuous thermal demagnetization that includes self-reversed remanence provides explanation for the presence of MTC. Extension of the model onto noncollinear primary (partially self-reversed) and secondary components can account for the difference between the results of stepwise and continuous thermal demagnetization of the Steens Mountain basalt from the B51 lava flow.

3. The physics of such difference is associated with magnetic memory that arises in grains with two interacting phases with markedly different Curie temperatures, irrespective of whether their interaction is positive or negative. In the discussed cases, the interaction is negative which shows up in complete or partial self-reversal of the respective remanence.

4. The presence of ferrimagnetic minerals (hemoilmenite or low-temperature oxidized titanomagnetite) of a certain composition that possess magnetic memory can interfere with the results of the conventional stepwise thermal demagnetiza-

tion. Therefore, reliable determination of paleo-directions in samples with such minerals requires additional studies. In this respect, agreement between the results of stepwise and continuous thermal demagnetization indicates that the directions are true. It they disagree, the true direction is that of characteristic remanence (ChRM) obtained by continuous thermal cleaning.

The study was supported by grants 15-35-20599, 15-05-06843, 16-35-60114 and 15-55-10055 from the Russian Foundation of Basic Research and by grant 14.Z50.31.0017 from the Government of the Russian Federation.

References

Burgess, S.D., Bowring, S.A., 2015. High-precision geochronology confirms voluminous magmatism before, during, and after Earth's most severe extinction. Science Advances 1 (7), e1500470. DOI: 10.1126/sciadv.1500470.

Coe, R.S., Prévot, M., Camps, P., 1995. New evidence for extraordinarily rapid change of the geomagnetic field during a reversal. Nature 374, 687–692.

Coe, R.S., Jarboe, N.A., Le Goff, M., Petersen, N., 2014. Demise of the rapid-field-change hypothesis at Steens Mountain: The crucial role of continuous thermal demagnetization. Earth Planet. Sci. Lett. 400, 302–312.

Eitel, M., Gilder, S., Kunzmann, T., Pohl, J., 2014. Rochechouart impact crater melt breccias record no geomagnetic field reversal. Earth Planet. Sci. Lett. 387, 97–106.

Fabian, K., Shcherbakov, V.P., McEnroe, S.A., 2013. Measuring the Curie temperature. Geochem. Geophys. Geosys. 14, 947–961.

Fabian, K., Williams, W., Shcherbakov, V., 2015. Finite element micromagnetic modeling of thermally activated magnetization processes. Geophys. Res. Abstracts 17, EGU2015-9845.

Fetisova, A.M., Veselovskiy, R.V., Latyshev, A.V., Radko, V.A., Pavlov, V.E., 2014. Magnetic stratigraphy of Permian–Triassic traps of the Kotui River valley (Siberian craton) in the light of new paleomagnetic data. Stratigrafiya. Geologicheskaya Korreliatsiya 22 (4), 36–51.

Gapeev, A.K., Tselmovich, V.A., 1988. Microstructure and composition of high-temperature-oxidized natural and synthetic titanomagnetite. Izv. AN SSSR, Fizika Zemli, No. 10, 42–49.

Khramov, A.N. (Ed.), 1982. Paleomagnitology [in Russian]. Nedra, Leningrad.

Krása, D., Shcherbakov, V., Kunzmann, T., Petersen, N., 2005. Self-reversal of remanent magnetization in basalts due to partially oxidized titanomagnetites. Geophys. J. Int. 162, 115–136.

Latyshev, A.V., Veselovskiy, R.V., Ivanov, A.V. Paleomagnetism of the Permian–Triassic intrusions from the Tunguska syncline and the Angara–Taseeva depression, Siberian Traps Large Igneous Province: evidence of contrasting styles of magmatism. Tectonophysics (in revision).

Mankinen, E.A., Prévot, M., Gromme, C.S., Coe, R.S., 1985. The Steens Mountain (Oregon) geomagnetic polarity transition 1. Directional history, duration of episodes, and rock magnetism. J. Geophys. Res. 90, 10,393–10,416.

McFadden, P.L., McElhinny, M., 1990. Classification of reversal test in paleomagnetism. Geophys. J. Int. 103, 725–729.

Mikhaltsov, N.E., Kazanskiy, A.Yu., Ryabov, V.V., Shevko, A.Ya., Kuprish, O.V., Bragin, V.Yu., 2012. Paleomagnetism of trap basalts in the northwestern Siberian craton, from core data. Russian Geology and Geophysics (Geologiya i Geofizika) 53 (11), 1228–1242 (1595–1613).

Nishitani, T., Kono, M., 1983. Curie temperature and lattice constant of oxidized titanomagnetite. Geophys. J. Roy. Astron. Soc. 74, 585–600.

Petersen, N., 1987. Observation of shrinkage cracks in ocean floor titanomagnetites. Phys. Earth Planet. Inter. 46, 197–205.

Prévot, M., Mankinen, E.A., Gromme, C.S., Coe, R.S., 1985. How the geomagnetic field vector reverses polarity. Nature 316, 230–234.

Prévot, M., Hoffman, K.A., Goguitchaichvili, A., Doukhan, J-C., Shcherbakov, V., Bina, V., 2001. The mechanism of self-reversal of thermoremanence in natural hemoilmenite crystals: new experimental data and model. Phys. Earth Planet. Inter. 126, 75–92.

Shcherbakov, V.P., Fabian, K., Sycheva, N.K., McEnroe, S.A., 2012. Size and shape dependence of the magnetic ordering temperature in nanoscale magnetic particles. Geophys. J. Int. 191, 954–964.

Shcherbakova, V.V., Shcherbakov, V.P., Heider, F., 2000. Properties of partial thermoremanent magnetization in PSD and MD magnetite grains. J. Geophys. Res. 105 (B1), 767–782.

Shipunov, S.V., 1999. Criteria of significance in paleomagnetism. Izv. RAN, Fizika Zemli, No. 6, 89–92.

Veselovskiy, R.V., Galle, I., Pavlov, V.E., 2003. Paleomagnetism of trap intrusions in the Podkamennaya Tunguska and Kotui River valleys: probability of post-Paleozoic relative motions of the Siberian and East European cratons. Izv. RAN, Fizika Zemli, No. 10, 78–94.

Vonsovskiy, S.V., 1971. Magnetism [in Russian]. Nauka, Moscow.

Wang, R.V., Mills, D.L., 1992. Onset of long-range order in superlattices: Mean-field theory. Phys. Rev. B 46 (18), 11,681–11,687.

Zijderveld, J.D.A., 1967. A.C. demagnetization of rocks: analysis of results, in: Collinson, D.W., Creer, K.M. (Eds.), Methods in Paleomagnetism. Elsevier, Amsterdam, pp. 254–286.

Editorial responsibility: D.V. Metelkin